Received: 10 April 2017 | Revised: 17 July 2017 | Accepted: 19 July 2017

DOI: 10.1002/nbm.3791

WILEY NMR IN BIOMEDICINE

RESEARCH ARTICLE

Accelerated 4D self-gated MRI of tibiofemoral kinematics

Valentina Mazzoli[1,2,3] | Jasper Schoormans[4] | Martijn Froeling[5] | Andre M. Sprengers[2,6] | Bram F. Coolen[4] | Nico Verdonschot[2,6] | Gustav J. Strijkers[3,4] | Aart J. Nederveen[1]

[1] Department of Radiology, Academic Medical Center, Amsterdam, the Netherlands

[2] Orthopedic Research Laboratory, Radboud University Medical Center, Nijmegen, the Netherlands

[3] Biomedical NMR, Department of Biomedical Engineering, Eindhoven University of Technology, Eindhoven, the Netherlands

[4] Department of Biomedical Engineering and Physics, Academic Medical Center, Amsterdam, the Netherlands

[5] Department of Radiology, University Medical Center, Utrecht, the Netherlands

[6] Laboratory for Biomechanical Engineering, University of Twente, Enschede, the Netherlands

Correspondence
V. Mazzoli, Department of Radiology, Academic Medical Center, Meibergdreef 9, 1105 AZ, Amsterdam the Netherlands.
Email: v.mazzoli@amc.uva.nl

Funding information
European Union COST Action, Grant/Award Number: BM1304; European Union's Seventh Framework Programme (FP/2007-2013)/ERC, Grant/Award Number: 323091; Dutch Technology Foundation STW, Grant/Award Number: #14348

Anatomical (static) magnetic resonance imaging (MRI) is the most useful imaging technique for the evaluation and assessment of internal derangement of the knee, but does not provide dynamic information and does not allow the study of the interaction of the different tissues during motion. As knee pain is often only experienced during dynamic tasks, the ability to obtain four-dimensional (4D) images of the knee during motion could improve the diagnosis and provide a deeper understanding of the knee joint. In this work, we present a novel approach for dynamic, high-resolution, 4D imaging of the freely moving knee without the need for external triggering. The dominant knee of five healthy volunteers was scanned during a flexion/extension task. To evaluate the effects of non-uniform motion and poor coordination skills on the quality of the reconstructed images, we performed a comparison between fully free movement and movement instructed by a visual cue. The trigger signal for self-gating was extracted using principal component analysis (PCA), and the images were reconstructed using a parallel imaging and compressed sensing reconstruction pipeline. The reconstructed 4D movies were scored for image quality and used to derive bone kinematics through image registration. Using our method, we were able to obtain 4D high-resolution movies of the knee without the need for external triggering hardware. The movies obtained with and without instruction did not differ significantly in terms of image scoring and quantitative values for tibiofemoral kinematics. Our method showed to be robust for the extraction of the self-gating signal even for uninstructed motion. This can make the technique suitable for patients who, as a result of pain, may find it difficult to comply exactly with instructions. Furthermore, bone kinematics can be derived from accelerated MRI without the need for additional hardware for triggering.

KEYWORDS
bone kinematics, cine MRI, compressed sensing, dynamic MRI, knee, principal component analysis

1 | INTRODUCTION

Although anatomical magnetic resonance imaging (MRI) is the most commonly used imaging technique for the evaluation and assessment of the knee joint, it does not provide dynamic information and therefore does not allow the study of the interaction of the different tissues during motion tasks.

The normal mechanism of motion in the tibiofemoral joint depends on both static and dynamic factors. Dynamic interaction between the different tissues during motion plays a fundamental role in the stability of the knee joint. For instance, one of the main dynamic stabilizers of the patella is the quadriceps muscle group. As a result of the fundamental role of the musculature in the biomechanical behavior of the patella, active quadriceps contraction is required to obtain a realistic assessment. This implies that a series of static images is not appropriate for the description of the real kinematic behavior. The added value of dynamic imaging has been shown by d'Entremont et al.,[1] who compared dynamically acquired MRI datasets with a series of static scans at different knee positions, and found significant differences in kinematic parameters. Furthermore, dynamic

Valentina Mazzoli and Jasper Schoormans contributed equally to this work.

Abbreviations used: 2D, two-dimensional; 3D, three-dimensional; 4D, four-dimensional; ACL, anterior cruciate ligament; ANCOVA, analysis of covariance; CNR, contrast-to-noise ratio; FFE, fast field echo; FFT, fast Fourier transform; PC, phase contrast; PCA, principal component analysis; PCL, posterior cruciate ligament; PD, proton density; SNR, signal-to-noise ratio; TSE, turbo spin echo; TTL, transistor-transistor logic; ZIP, z intensity-weighted position

MRI of the musculoskeletal system could provide information beyond static imaging to understand the cause of pain. Pain is often absent in static conditions and only present during a specific movement, as is often the case with impingements, for example. The ability to perform this specific movement inside the MRI scanner could provide the radiologist with additional tools to understand the cause of pain and to adapt the treatment accordingly.[2,3]

Fluoroscopy[4] has been proposed as a powerful method to study bone kinematics. Unlike MRI, it can provide bone kinematics under physiologically relevant loading conditions and during daily motion tasks. However, as it requires ionizing radiation, it is not an ideal candidate for longitudinal studies. Furthermore, fluoroscopy provides very limited soft tissue contrast, thus preventing the study of the interaction of the different soft tissue structures during motion.

MRI has been proposed as an alternative technique to assess tibiofemoral kinematics. Unlike fluoroscopy, it does not make use of ionizing radiation and allows for the visualization of soft tissues, such as the cartilage and muscles. Draper et al.[5,6] have assessed patellar tilt in patellofemoral dislocation using single-slice, real-time MRI. Although a real-time approach is desirable, it does not allow for volumetric imaging and thus does not provide three-dimensional (3D) information. Joint motion can also be visualized by phase contrast (PC)-CINE (synchronized) techniques.[7-9] These methods rely on the acquisition of a high-resolution static scan and three single-slice dynamic scans. Although bone kinematics can be accurately determined using this approach, it is intrinsically unsuitable for the 3D visualization of soft tissue motion. Furthermore, as PC techniques encode velocity, they require integration to obtain displacement, which is a procedure prone to error.

Kaiser et al. have developed a four-dimensional (4D) MRI technique to study tibiofemoral kinematics in healthy subjects[10] and in patients after anterior cruciate ligament (ACL) reconstruction.[11] After ACL reconstruction altered kinematic parameters were measured in comparison with the contralateral healthy knee. Abnormal kinematic parameters are believed to induce abnormal cartilage loading patterns, which could be a primary cause of osteoarthritis. Therefore, there is great clinical interest in tools that quantify knee kinematic parameters. Kaiser et al. acquired data using a 3D radial *k*-space encoding scheme. During data acquisition, the knee flexion angle was constantly externally monitored and this information was used for retrospective sorting of *k*-space spokes into a desired number of 3D frames.[10]

3D radial methods offer highly incoherent sampling of *k*-space, which is highly beneficial for compressed sensing reconstruction, and are inherently insensitive to motion artifacts within a given 3D time frame. However, eddy current-related artifacts pose a challenge and the image reconstruction is a computationally expensive process.

Stack-of-stars is an alternative 3D MRI acquisition scheme which consists of a radial sampling pattern in the k_x–k_y plane, and a Cartesian encoding in the k_z direction. Like 3D radial sampling, it is robust to motion artifacts,[12] and appropriate for undersampling and compressed sensing reconstruction. The stack-of-stars has some added benefits relative to 3D radial sampling: a reduced sampling time (pi/2 times fewer sampling points are required for a fully sampled image), and easier correction strategies for eddy current effects.[13] Furthermore, the Cartesian encoding in the stack direction enables different slices to be reconstructed in parallel, therefore greatly reducing the computation times. An advantage of stack-of-stars over cartesian encoding is that each readout for the central slice encoding passes through the center of *k*-space, thus facilitating retrospective self-gating,[14] and eliminating the need for external sensors and/or navigators.

Radial trajectories can be acquired following a golden angle ordering scheme,[15] in which the angle between two consecutive radial spokes is increased by 111.246°. This approach allows an almost uniform coverage of *k*-space to be obtained for a given number of consecutive spokes, which has the advantage of allowing continuous data acquisition and retrospective sorting of the spokes into several motion frames. The uniform distribution of the spokes using a golden angle ordering scheme allows for the reconstruction of an almost arbitrary number of time frames, thus offering high flexibility in terms of temporal resolution.

For dynamic MRI studies, the knee motion can either be externally imposed, making it less suitable for the assessment of contributions from active muscle contraction in the kinematics,[1] or be based on visual/audio instructions, synchronized with an external TTL (transistor-transistor logic) trigger. The latter approach relies heavily on the perfect execution of the motion task, which becomes problematic if the subject is not able to comply with instructions because of poor coordination skills or pain. An alternative approach is the use of an external sensor to continuously monitor the position of the leg in the scanner.[10] However, this requires additional hardware which is not standardly available with clinical MRI scanners.

In this study, we have developed a self-gated 4D stack-of-stars protocol to facilitate 4D imaging of the knee during flexion and extension. We have performed measurements in healthy volunteers during synchronized as well as free uninstructed movement of the knee, compared image quality and quantified the derived tibiofemoral kinematics. In addition to dynamic bone imaging, we show the feasibility of the technique for dynamic visualization of soft tissue structures in the knee.

2 | METHODS

2.1 | Subjects

We collected images of the dominant knee of five healthy female volunteers (age, 28 ± 1 years; weight, 61 ± 6 kg; body mass index, 22 ± 3 kg/m^2). None of the subjects had a history of knee injury or knee pain. We received informed consent from all the subjects prior to the study, according to our institution's regulations.

2.2 | Knee motion

The subjects were placed supine on the scanner table, with a triangular-shaped support underneath the knee, and were asked to perform a knee flexion/extension task. Two sand bags were placed laterally on each side of the knee in order to prevent sliding and rotation of the knee during the motion task. Three different experiments were performed for each subject: in the first two experiments, the subjects were asked to flex and extend their knee for about 5 min at a frequency of 0.67 Hz. In order to improve the repeatability and consistency of the motion task, the subjects were shown a video of a ball bouncing up and down with the required frequency whilst inside the scanner, and were asked to follow the movement of the ball ('*with instructions*'). Prior to the start of the experiments, the subjects were instructed to always touch the support when in the most flexed position, and to extend their knees until the edge of the bore was reached. Consequently, the amount of knee flexion was dependent on the size of the subject, but was kept relatively constant between different repetitions of the motion task for each subject. In order to simulate the effect of poor motor coordination skills, a third experiment was performed without constraints on the frequency of motion. For this experiment, no instruction was shown and the subjects were asked to move at their preferred pace ('*without instructions*'). For all experiments, the subjects flexed and extended their knees without any external weight.

2.3 | Image acquisition

MRI image acquisition was performed with a 3T Philips Ingenia scanner (Philips, Best, the Netherlands). All acquisitions were performed using a custom-built, 15-channel flexible coil array (MR Coils BV, Zaltbommel, the Netherlands). The coil array (3 × 5) was placed around the knee with Velcro straps and centered around the patella. The scan protocol consisted of five different datasets: two high-resolution anatomical datasets to be used for segmentation, and three dynamic scans during the knee movement tasks described previously.

The first high-resolution anatomical scan was a turbo spin echo (TSE) scan with proton density (PD) contrast (TR = 1000 ms; TE = 29.9 ms; scan time, 8 min). The second anatomical scan was a fast field echo (FFE) with ProSet fat suppression (TR = 10 ms; TE = 4.5 ms; scan time, 6 min). Both scans had a reconstructed matrix size of 352 × 352 × 230, and 0.68 × 0.68 × 0.7 mm^3 resolution.

The dynamic scans were obtained using a golden angle stack-of-stars sequence. A spoiled gradient echo sequence was used for data acquisition. Sequence parameters were as follows: matrix size, 160 × 160 × 47; voxel size, 1.5 × 1.5 × 3 mm^3; field of view, 240 × 240 × 141 mm^3; TE/TR = 1.3/3.9 ms. For Experiment 1, a flip angle of 20° was used to obtain high signal-to-noise ratio (SNR) from the bones. For Experiment 2, the same imaging sequence was used, with a flip angle of 5°, to enhance signal from collagen-rich structures, such as ligaments and cartilage. For Experiment 3 (movement '*without instructions*'), a flip angle of 20° was used. The acquisition was performed with 47 radial stacks with 1.3× slice oversampling. A *zy* ordering approach was used for the spoke acquisition, meaning that, for each radial angle, spokes from all stacks were acquired before advancing to the next radial angle. A total of 1410 spokes was acquired for each stack, with a tiny golden angle increment of 20.89°. A tiny golden angle increment was used instead of 111.246° in order to reduce eddy current effects, which could lead to artifacts in the reconstructed images.[16] Data were continuously acquired during 5 min 20 s of knee flexion/extension. All static and dynamic scans were acquired with readout in the sagittal orientation.

2.4 | Image reconstruction

The main steps used in the reconstruction process are summarized in Figure 1. Raw scan data were exported and post-processed with MRecon (Gyrotools, Zürich, Switzerland) and Matlab (The Mathworks Inc., Natick, MA). We applied a coil channel compression routine, reducing the number of channels from 24 (15 channels flexible coil +8 channels embedded in the scanner table + body coil) to 10 virtual channels.[17] Eddy current correction was performed offline.[13,18] An inverse fast Fourier transform (FFT) was applied along the fully sampled *z* dimension, resulting in a set of two-dimensional (2D) *k*-spaces which could be reconstructed in parallel.[14]

The synchronization signal required for self-gating was derived from the center of *k*-space after FFT in the *z* dimension. A principal component analysis (PCA) was calculated on the data matrix from the *k*-space center of the middle three slices of 10 channels and 1410 spokes (rows). The matrix on which PCA was performed had a size of 30 × 1410, corresponding to three slices in 10 channels (rows) and 1410 radial spokes (columns). All principal components were analyzed. We selected the principal components with the highest signal power in the frequency bands 0.6–0.75 Hz and 0.45–0.9 Hz for the instructed and non-instructed motion, respectively.[14] Next, the self-gating signal was filtered with a bandpass filter to suppress additional periodic signals of no interest (such as the rotational frequency in *k*-space). The cutoff frequencies for the bandpass filter were the upper and lower values of the corresponding frequency bands.

Subsequently, a peak-finding algorithm was applied to the filtered self-gating signal to define a fixed time point in each motion cycle. This was used to sort the measured spokes into 20 motion states, each with an equal number of *k*-space spokes. This resulted in 20 *k*-space frames containing 70 randomly angled spokes each, which corresponds to an undersampling factor of 3.59 (with respect to a fully sampled radial acquisition).

A parallel imaging, compressed sensing reconstruction was performed using the BART toolbox (https://github.com/mrirecon/bart/releases/tag/v0.3.01). Relevant parameters were as follows: total variation L1 regularization, (regularization parameter = 0.01, in the temporal and three spatial dimensions) and 100 iterations. Image reconstruction were performed in parallel for all slices. Dynamic sensitivity maps used for the reconstruction were estimated using the ESPIRiT method.[19] Sensitivity map estimation was performed for each dynamic frame independently, based on a sliding windows approach, in which the sensitivity map of frame *m* was constructed using *k*-space lines from frame *m* − 1, *m*, and *m* + 1. The average

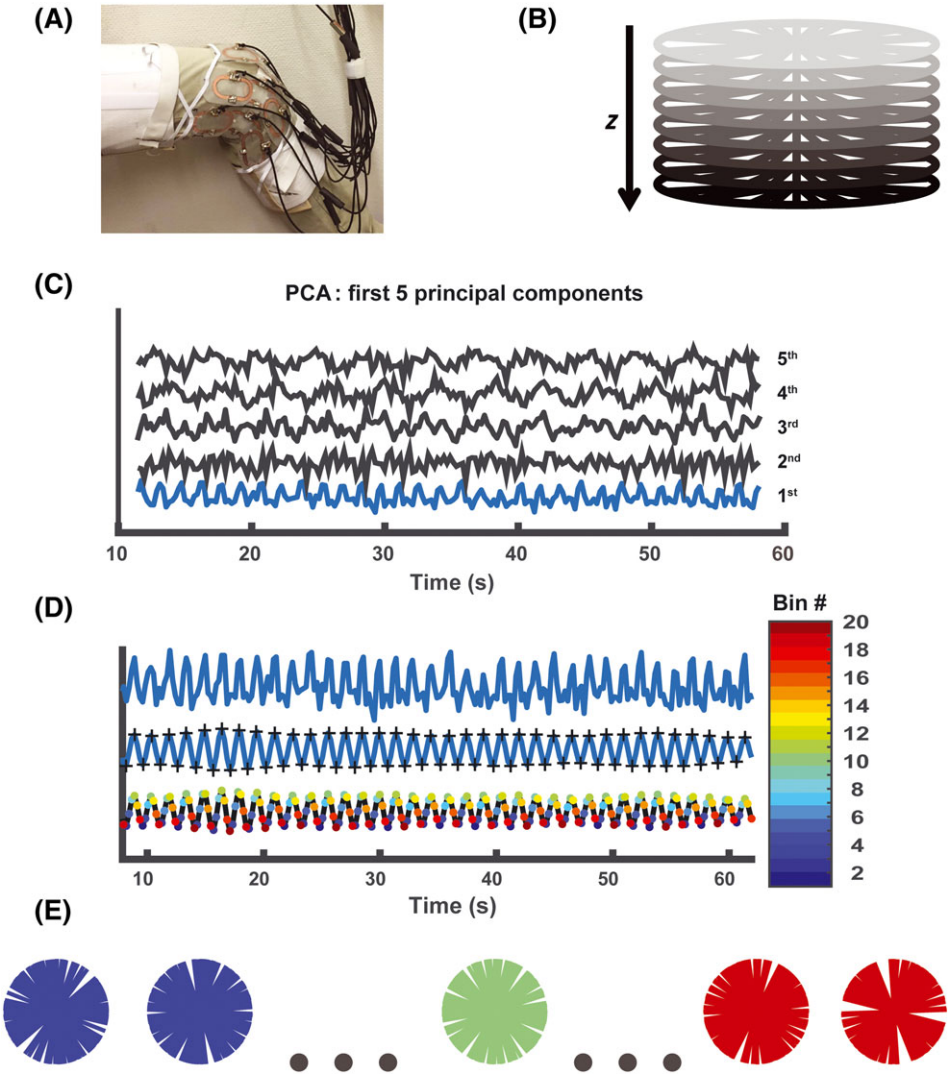

FIGURE 1 Schematic overview of the image acquisition and reconstruction pipeline. All images were acquired using a 15-channel, custom-built coil that could be wrapped around the subject's knee, offering high signal-to-noise ratio (SNR) without hindering the flexion/extension range of motion (a). A stack-of-stars sampling scheme was used (b). The three center stacks were used to determine the gating signal, based on principal component analysis. The first five principal components are shown in (c), from bottom to top. The first component, depicted in blue, represents the knee motion frequency. This component is filtered (d, middle row) and, after detection of the minima and maxima, is used to correctly assign each radial spoke to a given time bin (d, bottom row). The 20 sorted *k*-spaces, which were used to reconstruct 20 time frames, have an equal number of uniformly distributed spokes (e)

reconstruction time for a dataset was 3 h on a server with two Intel Xeon E5–2690 processors and 256GB RAM. The reconstruction resulted in a set of 20 3D images for each single flexion extension cycle.

2.5 | Image scoring

The movies obtained with and without instructions (Experiment 1 and Experiment 3) were scored in a blind fashion by two independent musculoskeletal MR imaging experts for sharpness, contrast, bone visibility, fluency of motion, and presence of artifacts. The scores were assigned on a scale from 0 to 3, where 0 was insufficient and 3 was of diagnostic quality. One-way analysis of covariance (ANCOVA) was used to compare the scoring obtained for the movies with instructions and without instructions. The reviewer was set as a covariate and $p < 0.05$ was considered to be significant.

2.6 | Image segmentation

The femur and the tibia of the five volunteers were segmented from the high-resolution FFE scan using a semiautomatic algorithm based on region growing (ITK-snap[20]). The contours were manually adjusted where necessary using the high-resolution, PD-weighted scan as an additional reference.

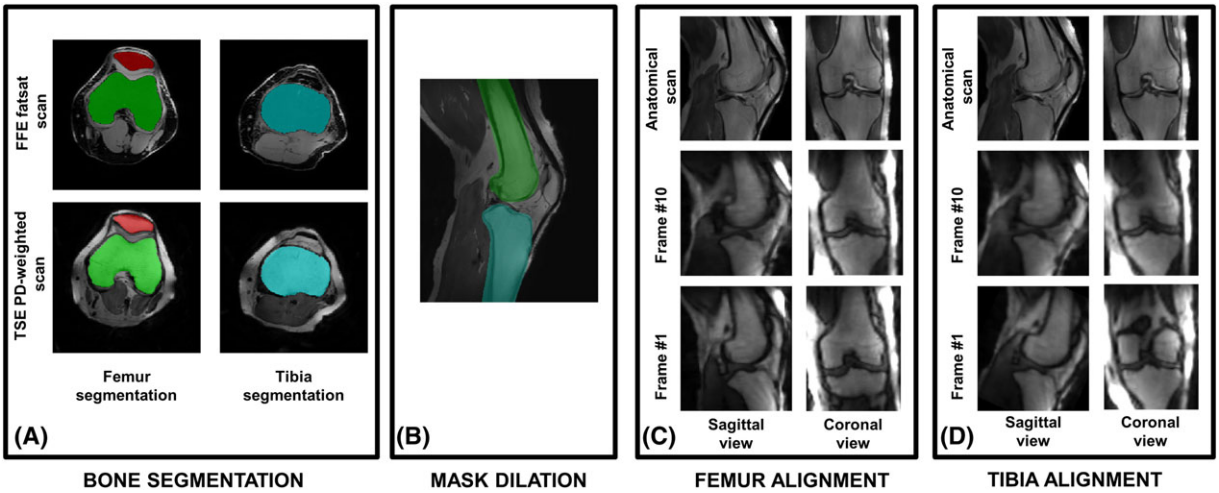

FIGURE 2 Image registration pipeline used to derive tibiofemoral kinematics from the reconstructed four-dimensional (4D) images. (A) three-dimensional (3D) bone masks are segmented from the high-resolution anatomical scans. (B) bone masks are slightly dilated, in order to contain the interface between bones and other tissues (muscle and fat). (C) rigid registration is performed with constraints on the femur, using the anatomical proton density (PD)-weighted scan as target. The result is a series of dynamic scans in which the femur is fixed. (D) a second rigid registration step is performed with constraints on the tibia. The first time frame of the previously determined dataset with a fixed femur was used as registration target. The result is a series of dynamic scans in which the tibia is fixed. The registration parameters of the last registration steps represent the tibiofemoral kinematics (three rotations and three translations)

2.7 | Determination of bone kinematics

After image reconstruction, a 3D registration pipeline was applied to the datasets obtained from Experiment 1 and Experiment 3 to determine the bone kinematics. The main registration steps are summarized in Figure 2. We used a rigid registration pipeline implemented in Elastix,[21] with 500 iteration steps and two levels of resolution. First, the segmented bone masks were convolved with a Gaussian kernel, and then dilated by a $3 \times 3 \times 3$ cubic voxel to increase their volume. The dilation of the masks was needed in order to include the interface between the bone and the adjacent tissues into the registration target, which is the primary feature that drives the registration of the dynamic datasets. Subsequently, the dynamic datasets were reformatted to an isotropic resolution of $1.5 \times 1.5 \times 1.5$ mm^3. The femur in the first dynamic frame was registered to the femur in the PD-weighted scans. The registered frame was used as a registration target for the subsequent 19 dynamic frames over the motion cycle. The results of this registration step were 20 time frames with a static femur, and a moving tibia. An automated selection routine based on minimum detection of the femur translation curve was applied to this dataset to define the first time frame in a consistent way across the volunteers. This corresponded to the knee in full flexion. After femur registration, the same pipeline was repeated for the tibia, using the images with the registered femur as target.

The final result was a set of rigid body trajectories (three rotations and three translations) of the tibia with respect to the femur over the full motion cycle (20 dynamic frames). For each volunteer, the center of rotation was defined in the center of mass of the high-resolution anatomical scan used for segmentation and the axis parallel to the axis of the image. The angles presented refer to the roll, pitch and yaw convention, with rotations performed in the order roll, yaw and pitch. All kinematic trajectories were subsequently smoothed using a Gaussian filter with a smoothing factor of two. Differences between the peak kinematic values measured at time frame #10 (at which peak flexion occurred in all the subjects), with and without instructions, were statistically evaluated using a paired t-test, where $p < 0.05$ was considered to be significant.

3 | RESULTS

All volunteers were able to perform the motion task very consistently when instructed via a visual cue, which is illustrated by the narrow peak in the frequency spectrum of the self-gating signal (Figures 3a and 4a). The typical spectra derived from the first principal component for instructed motion are shown in Figure 3a (before filtering) and Figure 3b (after the application of a bandpass filter) for one of the volunteers. However, for uninstructed motion, a worse repeatability of the motion task was observed in the same volunteer, as indicated by the broadening of the motion peak in Figure 3c (before filtering) and Figure 3d (after the application of a bandpass filter). Figure 4a,b shows the mean self-gating signal averaged over the five volunteers. The agreement between the visual cue frequency and the self-gating frequency spectra of all volunteers for instructed motion (Figure 4a) indicates a credible self-gating signal. Without a visual cue, the peak of the motion frequency was different for the different volunteers (Figure 4b) and the peak broadened, indicating a larger variability in motion during the approximately 5-min acquisition (Figure 4b,c). However, in both cases, the self-gating approach based on PCA allowed for a correct assignment of the motion states, resulting in 3D movie frames of high quality without significant motion-related blurring and artifacts (Figure 5). There was no significant difference in the expert image scores for the movies reconstructed from the instructed and uninstructed acquisitions (Table 1).

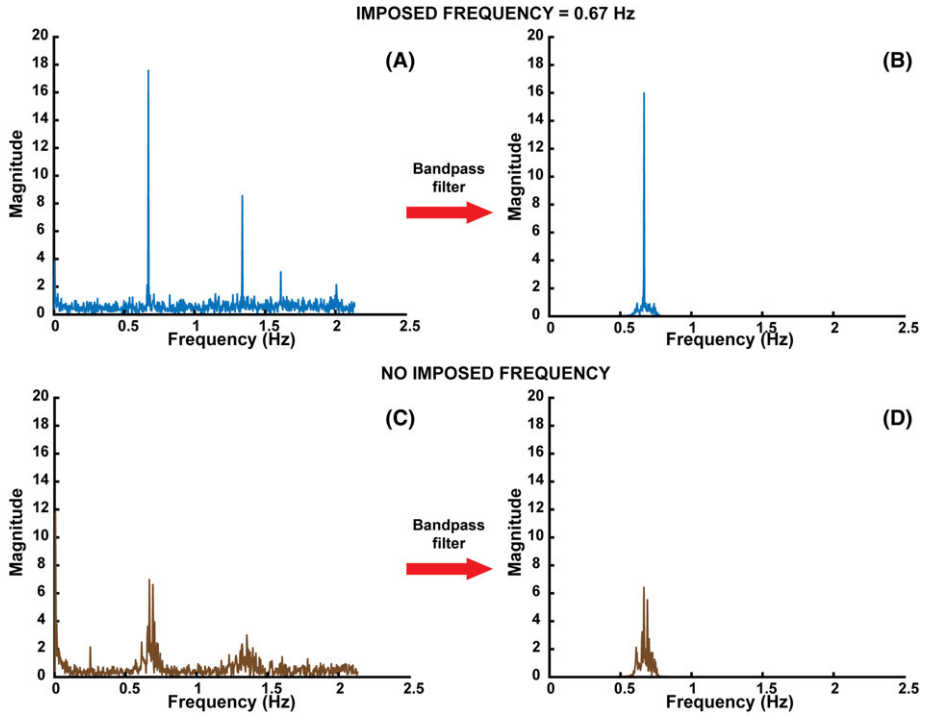

FIGURE 3 First principal component for one volunteer before (A) and after (B) filtering with a bandpass filter. The main peak corresponds to the frequency of the visual cue (0.67). When no visual cue is provided, a typical broadening of the motion peak is observed (C and D, before and after filtering, respectively). The filtered spectra, shown in (B) and (D), are used as self-gating signals

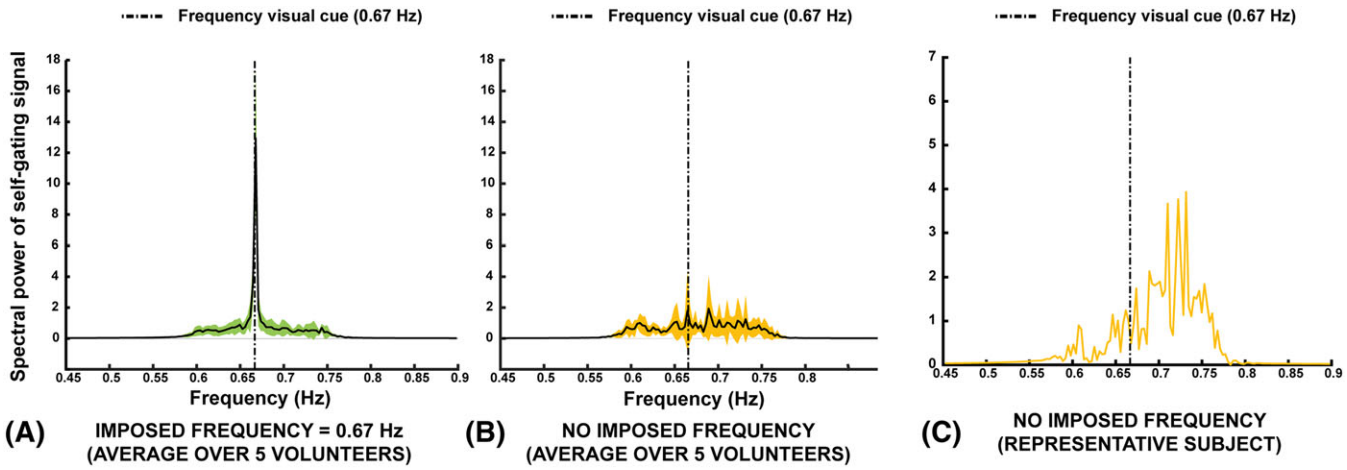

FIGURE 4 Mean self-gating signal, averaged over the five volunteers, when instructions were given using a visual cue (A) and when the motion task was performed without instructions (B). The frequency of the visual cue, corresponding to 0.67 Hz, is indicated as the dotted line for reference in (A–C), although the visual cue was only used to acquire the data in (A). (C) representative motion spectrum for one of the volunteers. In this case, the frequency peak appears to be broader and at average higher frequency, suggesting that the motion task performed without instruction could be a good way to simulate the motion task performed by an orthopedic patient

The ranges of knee flexion achieved in the scanner by the subjects were 16.2° ± 1.7° (motion *with instructions*) and 14.5° ± 3.0° (motion *without instructions*) averaged over the five subjects. The kinematic parameters representing tibiofemoral motion are presented in Figure 6.

A small tibial external/internal rotation was measured for all subjects with increasing flexion angle. The peak tibial internal rotations across subjects were 3.4° ± 1.9° (motion *with instructions*) and 2.8° ± 2.6° (motion *without instructions*). Larger inter-subject variation was detected for the translational degrees of freedom, as compared to the rotational degrees of freedom.

Taken together, the three rotational and three translational values and their variability, which describe the full range of possible tibiofemoral motions during knee flexion and extension, were similar for instructed and uninstructed tasks. The mean values for each kinematic parameter were calculated at frame #10, which corresponds to the knee in maximum flexion. The results are presented in Figure 7. A paired *t*-test revealed no differences between the results obtained with and without instructions ($p > 0.17$).

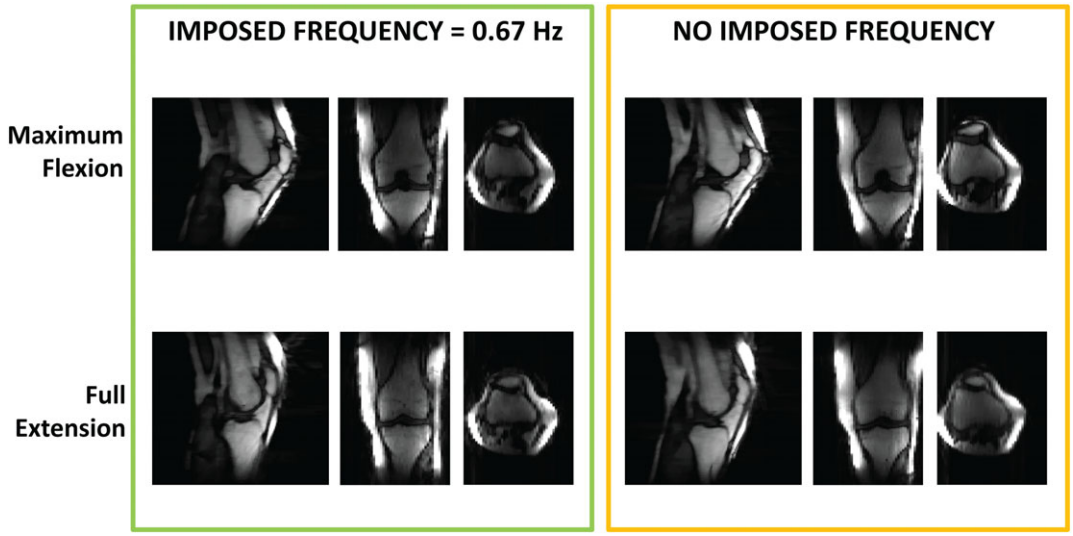

FIGURE 5 Two reconstructed dynamic frames (out of 20) representing the maximum achieved flexion and the full extension for a volunteer. Sagittal, coronal and transverse views are presented. The left images were acquired when the subject was instructed to move at 0.67 Hz, whereas, during the acquisition of the right images, the subjects were free to move at their own preferred pace. For both datasets, the flip angle was 20°

TABLE 1 Results of scoring of the four-dimensional (4D) movies by two musculoskeletal imaging experts. The scores were assigned on a scale from 0 to 3. No statistical difference ($p > 0.05$) was observed in terms of sharpness, contrast, bone visibility, fluency of motion and presence of artifacts with the instructed frequency of 0.67 Hz ('*with instructions*') relative to free movement ('*without instructions*')

Criteria	With instructions	Without instructions	p
Sharpness	2.2	2.1	0.721
Contrast	2.3	2.2	0.692
Bone visibility	2.2	2.3	0.703
Fluency of motion	3.0	2.9	0.331
Artifacts	2.0	1.9	0.668

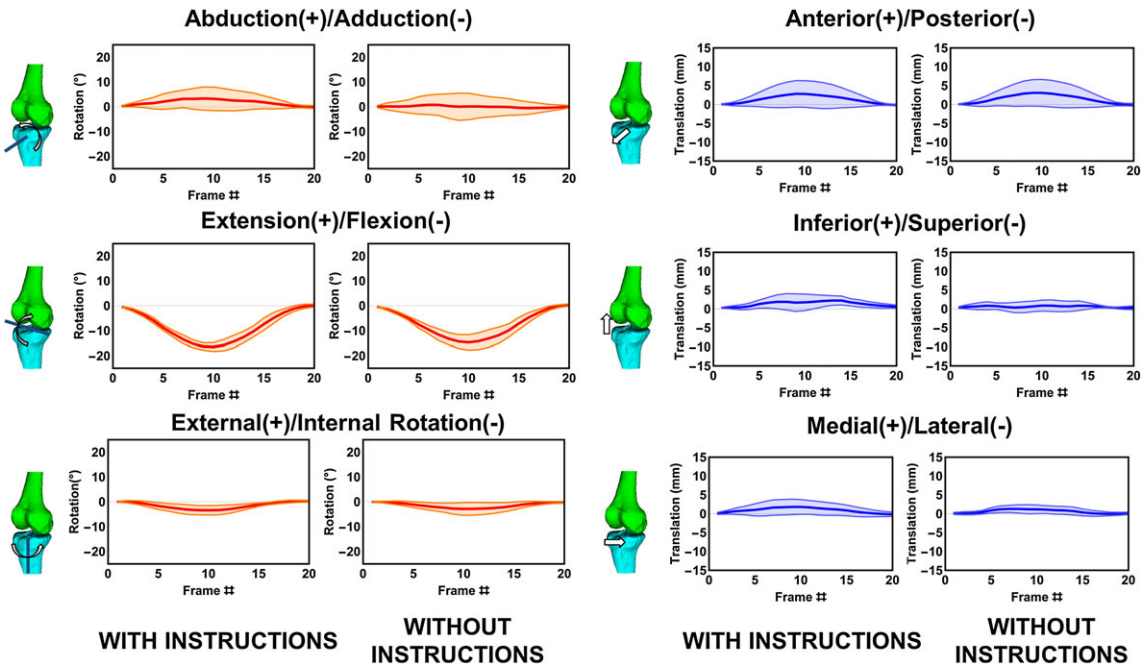

FIGURE 6 Tibiofemoral kinematics averaged over five healthy volunteers (shaded curves represent mean ± standard deviation) as a function of frame number. The three rotational degrees of freedom (abduction/adduction, extension/flexion and external/internal rotation) are indicated in red. The three translational degrees of freedom (anterior/posterior, inferior/superior and medial/lateral translation) are indicated in blue. Similar curves were observed when the instructed frequency was 0.67 Hz ('*with instructions*') relative to free movement ('*without instructions*')

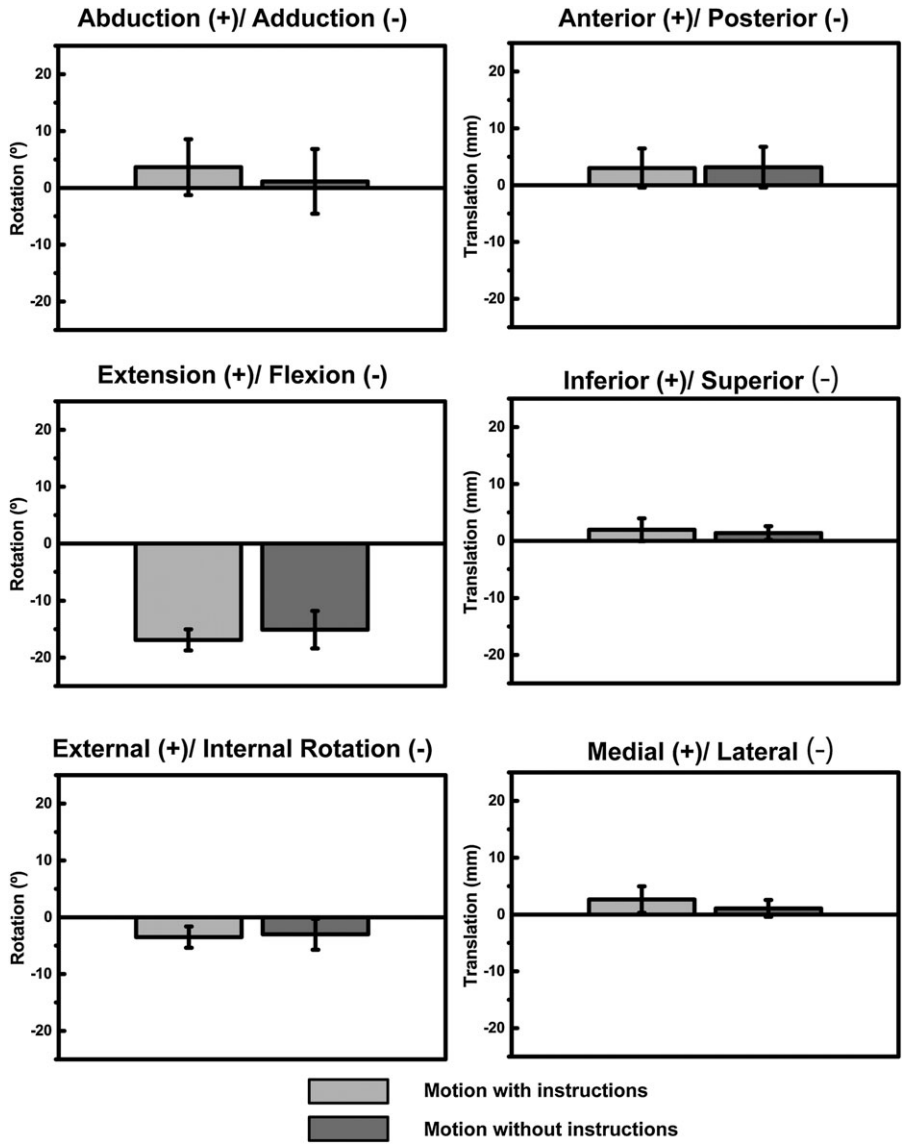

FIGURE 7 Bar graphs representing the tibiofemoral kinematics in the middle time frame (#10). Results are averaged over the five volunteers and the bars indicate standard deviation. No statistically significant differences were observed between the peak kinematic parameters obtained with (light gray) and without (dark gray) instructions

The use of a low flip angle resulted in higher signal from collagen-rich structures, such as ligaments and cartilage. In Figure 8, two time frames with the knee in maximum flexion and full extension are shown. The posterior cruciate ligament (PCL) presents high curvature in the extended position, and becomes progressively more stretched as a function of increasing knee flexion angle.

Representative 4D movies obtained for a volunteer moving with and without instructions are presented in Videos S1 and S2 (see Supporting Information), respectively, together with the movie obtained with instructions and the low flip angle (Video S3).

4 | DISCUSSION

The proposed golden angle radial sequence enabled the acquisition of self-gating signals which were successfully used to bin the data into 20 time frames over the flexion/extension cycle of the knee. We tested the sequence in five female volunteers, who were instructed to keep a constant frequency of 0.67 Hz during motion. In addition, the volunteers were also asked to perform flexion extension without any visual instructions. We found no statistically significant differences in image quality scores between the two methods. Furthermore, we obtained similar results in terms of tibiofemoral kinematics extracted from the movies with and without instructions.

Self-gated MRI is gaining popularity for cardiac imaging,[22,23] as well as abdominal imaging,[24,25] to estimate motion in relation to radiotherapy treatment planning. The self-gating approach is very attractive as it allows binning of the data in several motion states based on the *k*-space itself without relying on external triggering devices. As the binning is performed retrospectively, the number of movie frames and the data undersampling factor can be chosen after data acquisition.

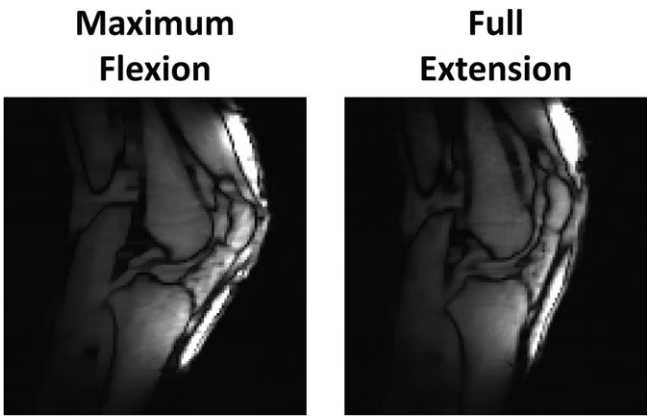

FIGURE 8 Two different reconstructed dynamic frames (out of 20) representing the maximum achieved flexion and the full extension for a volunteer during instructed motion at a frequency of 0.67 Hz. The flip angle used in the acquisition was 5°. The increasing stretching pattern of the posterior cruciate ligament for increasing flexion angle of the knee can be observed

A larger number of movie frames with increased data undersampling generally leads to lower SNR and more image artifacts, such as streaking. However, these artifacts can be reduced by compressed sensing image reconstruction.[14,26] In practice, a compromise must be reached between the temporal resolution and the presence of image reconstruction artifacts, as a small number of movie frames will result in motion blurring, and a large number of movie frames will lead to undersampling artifacts, even with compressed sensing reconstruction. We heuristically found that 20 frames over the flexion/extension cycle was the optimal trade off.

It should be understood that, with our technique, the motion is not depicted in real time, but, rather, averaged over several motion cycles. This is not a limitation specific to our particular approach, but, rather, inherently related to the fact that 3D MRI with sufficient spatial resolution is too slow for real-time imaging, even with state-of-the-art acceleration techniques. For the practical application of dynamic knee imaging, this implies that sudden movements, such as dislocations, cannot be visualized using a gated method. Therefore, a real-time method[27] is required, but this is currently limited to single-slice imaging.

Using our imaging method, in combination with novel image registration techniques, we were able to quantify the displacement of the tibia relative to the femur. The current gold standard for the determination of bone kinematics is biplane fluoroscopy. This technique allows the acquisition of functional information during physiologically relevant tasks, such as stair rising[4] and gait,[28] with very high temporal and spatial resolution. However, fluoroscopy involves the use of ionizing radiation, which makes its impractical for longitudinal studies, and requires highly specialized machines, which are not largely available in clinical settings. On the other hand, MRI scanners are present in virtually every hospital and are routinely used for the evaluation of the knee joint.

As we used a closed-bore scanner, we had to deal with a limited range of motion of the knee joint as a result of geometrical constraints. This limitation could be solved with the use of an open-bore[29] or a vertical MRI system[5], although at the expense of temporal and spatial resolution related to the typically lower field strength of these systems.

Previous studies have focused on the determination of normative patellofemoral and tibiofemoral kinematics using PC-MRI.[7,8] PC-MRI relies on velocity measurements over time, which can be integrated to provide displacement measurements. The technique proposed by Rebmann and Sheehan[8] is based on an unloaded flexion/extension task that is synchronized with an external trigger. As a result of the need to acquire velocity information along three orthogonal directions and the compliance of the subjects, the measurements are limited to three single-slice acquisitions of 2 min 48 s each (through the patella, femur and tibia). This technique heavily relies on the ability of the subject to maintain a constant motion frequency, and small imperfections in the execution of the task can result in spatial and temporal blurring of the velocity values that may lead to errors in the quantification of bone kinematics and even make the images unusable.

Although bone motion can also be evaluated precisely and with higher frame rate using dynamic CT,[30] the ability to simultaneously observe soft tissue and bone during motion makes our MRI-based approach unique. We were able to obtain images of the moving knee with relatively high resolution and sufficient soft tissue contrast, as indicated by the image scoring.

In this study, image scoring by experts was employed instead of more conventional SNR and contrast-to-noise ratio (CNR) measurements due to the use of compressed sensing reconstruction. In fact, when compressed sensing is used, high SNR can be obtained by simply increasing the regularization parameter, without any corresponding increase in image quality or diagnostic information.[31]

The images obtained with a low flip angle show high signal from ligaments and cartilage, potentially allowing the evaluation of these tissues during motion. The added value of dynamic imaging for soft tissue assessment in diagnosis still needs to be evaluated systematically, and spatial resolution will probably need to be improved in order to increase the usefulness of these images. Nonetheless, the preliminary results presented in this study are a first step towards the assessment of soft tissue motion in three dimensions.

In general, the lack of motion instructions resulted in a poorer repeatability of the task, as indicated by the lack of a well-defined frequency peak in this condition. Although this could lead to incorrect sorting of the *k*-space spokes in bins, the expert quality scoring of the movies from the instructed and uninstructed tasks was similar, suggesting that sorting was robust to non-repetitive motion. Although we believe that visual

(or auditory) guidance to motion should always be provided for dynamic MRI studies, conventional acquisition strategies based on prospective gating do not offer robustness against deviation from the given instructions. Many repetitions of the motion, especially under load, can lead to error in the executions of the task. Similarly, execution errors can be expected in orthopedic patients or subjects who, as a result of pain, may find it difficult to comply with instructions. Therefore, our self-gating method based on PCA and phase binning could be a useful tool for the evaluation of these subjects, especially during long and/or loaded acquisitions.

All of our acquisitions were obtained using a custom-built flexible knee coil, consisting of a 3 × 5 channel coil array. Although the coil added benefits in terms of SNR and image quality, our imaging pipeline is not hardware dependent and can be easily generalized to other anatomies (such as the wrist and ankle) and to other coil configurations.

Our self-gating signal was extracted from the three center slices of *k*-space. Other methods exist (i.e. z intensity-weighted position (ZIP)[32]). However, for our application and slice orientation, they proved unreliable. We performed phase binning, instead of magnitude binning often used in respiratory motion[33] because in our experiments, the volunteers were instructed to maintain fixed start and end points for the flexion extension task. In this situation, an almost fixed magnitude of motion was expected, but significant variation in the frequency could occur. Therefore, phase binning could be used more robustly than magnitude binning.

A general limitation of self-gating methods is that there is no absolute time stamp that indicates the beginning and end of the flexion and extension cycle. For image scoring by the experts, this was no problem, as movies were visualized in an infinite loop. However, the quantification of bone kinematics analysis requires a knowledge of the time frame of maximum flexion and extension. Here, we determined these time points by automatic detection of the minimum in the translation curve after the registration of the femur, and this represented the maximum achievable extension. The starting point was chosen to be the full extension position, as the bone position was relatively constant for all volunteers in full extension, whereas the maximum flexion position was largely dependent on the size of the subjects.

An additional limitation of our self-gating method is that it fails to determine the motion frequency when too much net translation of the knee occurs in the mediolateral direction. In our study, the problem was mitigated by placing sand bags on each side of the knee. In order to completely avoid this problem, a motion device should be designed that restricts the range of motion in the mediolateral direction, whilst allowing a full range of motion in the sagittal plane. Furthermore, a loading device could also increase the physiological values of the kinematic measurements, as compared with the 'no-load' condition applied in this study.

We did not define an anatomical frame of reference based on the tibia and the femur. Therefore, our kinematic results cannot be compared directly with previous studies.[7,8] The determination of an anatomical frame of reference based on bony landmarks could introduce additional inter-subject variation.[34] Therefore, for the purpose of this study, we preferred a direct comparison of the derived motions from the datasets obtained with and without instructions.

In conclusion, we have implemented a method to obtain self-gated 4D images of the moving knee using a golden angle radial sampling of *k*-space. Using a stack-of-stars sampling scheme, we were able to derive the trigger signal directly from the data, without the need for any external monitoring device. Compressed sensing allowed for high undersampling factor (3.59 fold), and the achieved scan time could allow the application of the technique an as addition to standard clinical protocols. Furthermore, we showed that high-resolution anatomical scans could be co-registered with the dynamic images to provide measurements of bone kinematics. Due to its simplicity, the method shows potential in the evaluation of knee structures during motion and to track *in vivo* skeletal kinematics non-invasively in a clinical setting.

ACKNOWLEDGEMENTS

The research leading to these results has received funding from the European Research Council under the European Union's Seventh Framework Programme (FP/2007-2013)/ERC Grant Agreement n. 323091 awarded to N. Verdonschot. We also received funding from the European Union COST Action BM1304, and from the Dutch Technology Foundation STW (VENI grant number 14348).

ORCID

Valentina Mazzoli http://orcid.org/0000-0002-6700-8424

REFERENCES

1. d'Entremont AG, Nordmeyer-Massner JA, Bos C, Wilson DR, Pruessmann KP. Do dynamic-based MR knee kinematics methods produce the same results as static methods? *Magn Reson Med*. 2013;69(6):1634-1644.
2. Gold GE. Dynamic and functional imaging of the musculoskeletal system. *Semin Musculoskelet Radiol*. 2003;7(4):245-248.
3. Shapiro LM, Gold GE. MRI of weight bearing and movement. *Osteoarthritis Cartilage*. 2012;20(2):69-78.
4. Akbarshahi M, Fernandez JW, Schache AG, Pandy MG. Subject-specific evaluation of patellofemoral joint biomechanics during functional activity. *Med Eng Phys*. 2014;36(9):1122-1133.
5. Draper CE, Besier TF, Santos JM, et al. Using real-time MRI to quantify altered joint kinematics in subjects with patellofemoral pain and to evaluate the effects of a patellar brace or sleeve on joint motion. *J Orthop Res*. 2009;27(5):571-577.
6. Draper CE, Besier TF, Fredericson M, et al. Differences in patellofemoral kinematics between weight-bearing and non-weight-bearing conditions in patients with patellofemoral pain. *J Orthop Res*. 2011;29(3):312-317.

7. Seisler AR, Sheehan FT. Normative three-dimensional patellofemoral and tibiofemoral kinematics: a dynamic, in vivo study. *IEEE Trans Biomed Eng*. 2007;54(7):1333-1341.
8. Rebmann AJ, Sheehan FT. Precise 3D skeletal kinematics using fast phase contrast magnetic resonance imaging. *J Magn Reson Imaging*. 2003;17(2):206-213.
9. Westphal CJ, Schmitz A, Reeder SB, Thelen DG. Load-dependent variations in knee kinematics measured with dynamic MRI. *J Biomech*. 2013;46(12):2045-2052.
10. Kaiser J, Bradford R, Johnson K, Wieben O, Thelen DG. Measurement of tibiofemoral kinematics using highly accelerated 3D radial sampling. *Magn Reson Med*. 2013;69(5):1310-1316.
11. Kaiser J, Vignos MF, Liu F, Kijowski R, Thelen DG. American Society of Biomechanics Clinical Biomechanics Award 2015: MRI assessments of cartilage mechanics, morphology and composition following reconstruction of the anterior cruciate ligament. *Clin Biomech*. 2016;34:38-44.
12. Glover GH, Pauly JM. Projection reconstruction techniques for reduction of motion effects in MRI. *Magn Reson Med*. 1992;28(2):275-289.
13. Buonincontri G, Methner C, Krieg T, Carpenter TA, Sawiak SJ. Trajectory correction for free-breathing radial cine MRI. *Magn Reson Imaging*. 2014;32(7):961-964.
14. Feng L, Axel L, Chandarana H, Block KT, Sodickson DK, Otazo R. XD-GRASP: golden-angle radial MRI with reconstruction of extra motion-state dimensions using compressed sensing. *Magn Reson Med*. 2016;75(2):775-788.
15. Winkelmann S, Schaeffter T, Koehler T, Eggers H, Doessel O. An optimal radial profile order based on the golden ratio for time-resolved MRI. *IEEE Trans Med Imaging*. 2007;26(1):68-76.
16. Wundrak S, Paul J, Ulrici J, Hell E, Rasche V. A small surrogate for the golden angle in time-resolved radial MRI based on generalized fibonacci sequences. *IEEE Trans Med Imaging*. 2015;34(6):1262-1269.
17. Buehrer M, Pruessmann KP, Boesiger P, Kozerke S. Array compression for MRI with large coil arrays. *Magn Reson Med*. 2007;57(6):1131-1139.
18. Moussavi A, Untenberger M, Uecker M, Frahm J. Correction of gradient-induced phase errors in radial MRI. *Magn Reson Med*. 2014;71(1):308-312.
19. Uecker M, Lai P, Murphy MJ, et al. ESPIRiT – an eigenvalue approach to autocalibrating parallel MRI: where SENSE meets GRAPPA. *Magn Reson Med*. 2014;71(3):990-1001.
20. Yushkevich PA, Piven J, Hazlett HC, et al. User-guided 3D active contour segmentation of anatomical structures: significantly improved efficiency and reliability. *Neuroimage*. 2006;31(3):1116-1128.
21. Klein S, Staring M, Murphy K, Viergever MA, Pluim JPW. Elastix: a toolbox for intensity-based medical image registration. *IEEE Trans Med Imaging*. 2010;29(1):196-205.
22. Motaal AG, Coolen BF, Abdurrachim D, et al. Accelerated high-frame-rate mouse heart cine-MRI using compressed sensing reconstruction. *NMR Biomed*. 2013;26(4):451-457.
23. Paul J, Divkovic E, Wundrak S, et al. High-resolution respiratory self-gated golden angle cardiac MRI: comparison of self-gating methods in combination with k-T SPARSE SENSE. *Magn Reson Med*. 2015;73(1):292-298.
24. Deng Z, Pang J, Yang W, et al. Four-dimensional MRI using three-dimensional radial sampling with respiratory self-gating to characterize temporal phase-resolved respiratory motion in the abdomen. *Magn Reson Med*. 2016;75(4):1574-1585.
25. Cruz G, Atkinson D, Buerger C, Schaeffter T, Prieto C. Accelerated motion corrected three-dimensional abdominal MRI using total variation regularized SENSE reconstruction. *Magn Reson Med*. 2015;1498:1484-1498.
26. Benkert T, Feng L, Sodickson DK, Chandarana H, Block KT. Free-breathing volumetric fat/water separation by combining radial sampling, compressed sensing, and parallel imaging. *Magn Reson Med*. 2016;576:565-576.
27. Mazzoli V, Nederveen AJ, Oudeman J, et al. Water and fat separation in real-time MRI of joint movement with phase-sensitive bSSFP. *Magn Reson Med*. 2017;78(1):58-68.
28. Guan S, Gray HA, Keynejad F, Pandy MG. Mobile biplane X-ray imaging system for measuring 3D dynamic joint motion during overground gait. *IEEE Trans Med Imaging*. 2016;35(1):326-336.
29. King AJ, Deng Q, Tyson R, et al. In vivo open-bore MRI reveals region- and sub-arc-specific lengthening of the unloaded human posterior cruciate ligament. *PLoS One*. 2012;7(11):1-10.
30. Carelsen B, Jonges R, Strackee SD, et al. Detection of in vivo dynamic 3-D motion patterns in the wrist joint. *IEEE Trans Biomed Eng*. 2009;56(4):1236-1244.
31. Feng L, Benkert T, Block KT, Sodickson DK, Otazo R, Chandarana H. Compressed sensing for body MRI. *J Magn Reson Imaging*. 2017;45:966-987.
32. Spincemaille P, Liu J, Nguyen T, Prince MR, Wang Y. Z intensity-weighted position self-respiratory gating method for free-breathing 3D cardiac CINE imaging. *Magn Reson Imaging*. 2011;29(6):861-868.
33. Han F, Zhou Z, Cao M, Yang Y, Sheng K, Hu P. Respiratory motion-resolved, self-gated 4D-MRI using rotating cartesian k-space (ROCK). *Med Phys*. 2017;44(4):1359-1368.
34. Morton NA, Maletsky LP, Pal S, Laz PJ. Effect of variability in anatomical landmark location on knee kinematic description. *J Orthop Res*. 2007;9:1221-1230.

SUPPORTING INFORMATION

Additional Supporting Information may be found online in the supporting information tab for this article.

How to cite this article: Mazzoli V, Schoormans J, Froeling M, et al. Accelerated 4D self-gated MRI of tibiofemoral kinematics. *NMR in Biomedicine*. 2017;30:e3791. https://doi.org/10.1002/nbm.3791